Aalto University

Aaltodoc
OPEN ACCESS

This is an electronic reprint of the original article.
This reprint may differ from the original in pagination and typographic detail.

Author(s): Niemelä, Janne-Petteri & Hirose, Yasushi & Hasegawa, Tetsuya & Karppinen, Maarit

Title: Transition in electron scattering mechanism in atomic layer deposited Nb:TiO2 thin films

Year: 2015

Version: Final published version

**Please cite the original version:**

Niemelä, Janne-Petteri & Hirose, Yasushi & Hasegawa, Tetsuya & Karppinen, Maarit. 2015. Transition in electron scattering mechanism in atomic layer deposited Nb:TiO2 thin films. Applied Physics Letters. Volume 106, Issue 4. 042101/1-4. ISSN 0003-6951 (printed). DOI: 10.1063/1.4906865.

Rights: © 2015 AIP Publishing. This article may be downloaded for personal use only. Any other use requires prior permission of the authors and the American Institute of Physics. The following article appeared in Applied Physics Letters. Volume 106, Issue 4 and may be found at http://scitation.aip.org/content/aip/journal/apl/106/4/10.1063/1.4906865.

All material supplied via Aaltodoc is protected by copyright and other intellectual property rights, and duplication or sale of all or part of any of the repository collections is not permitted, except that material may be duplicated by you for your research use or educational purposes in electronic or print form. You must obtain permission for any other use. Electronic or print copies may not be offered, whether for sale or otherwise to anyone who is not an authorised user.

AIP | Applied Physics Letters

# Transition in electron scattering mechanism in atomic layer deposited Nb:TiO2 thin films

Janne-Petteri Niemelä, Yasushi Hirose, Tetsuya Hasegawa, and Maarit Karppinen

Citation: Applied Physics Letters **106**, 042101 (2015); doi: 10.1063/1.4906865
View online: http://dx.doi.org/10.1063/1.4906865
View Table of Contents: http://scitation.aip.org/content/aip/journal/apl/106/4?ver=pdfcov
Published by the AIP Publishing

**Articles you may be interested in**

Limits of carrier mobility in Sb-doped SnO2 conducting films deposited by reactive sputtering
APL Mat. **3**, 062802 (2015); 10.1063/1.4916586

Highly transparent Nb-doped indium oxide electrodes for organic solar cells
J. Vac. Sci. Technol. A **32**, 021202 (2014); 10.1116/1.4832238

Effect of niobium doping on the optical and electrical properties in titanium dioxide grown by pulsed laser deposition
J. Vac. Sci. Technol. B **30**, 050603 (2012); 10.1116/1.4750373

Transparent semiconducting Nb-doped anatase TiO 2 films deposited by helicon-wave-excited-plasma sputtering
J. Vac. Sci. Technol. B **29**, 011017 (2011); 10.1116/1.3525918

Electrical and optical properties of Nb-doped TiO 2 films deposited by dc magnetron sputtering using slightly reduced Nb-doped TiO 2 − x ceramic targets
J. Vac. Sci. Technol. A **28**, 851 (2010); 10.1116/1.3358153

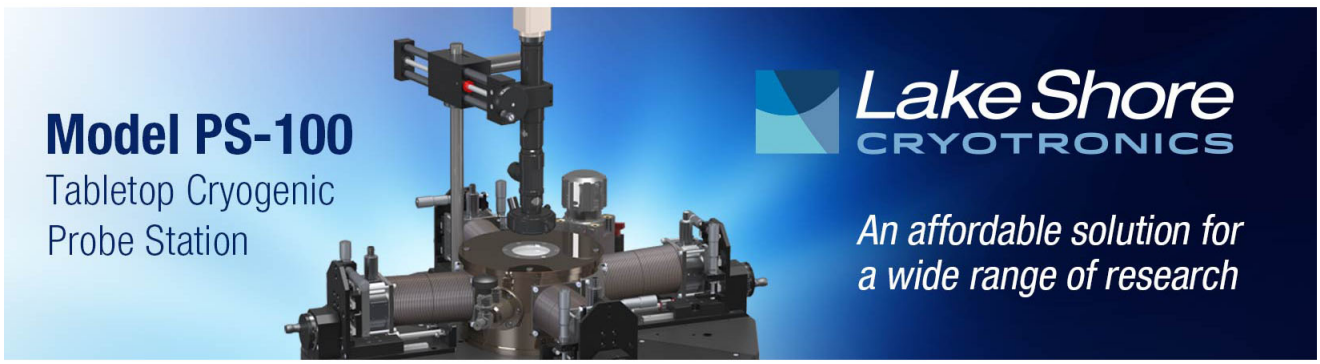


This article is copyrighted as indicated in the article. Reuse of AIP content is subject to the terms at: http://scitation.aip.org/termsconditions. Downloaded to IP: 130.233.216.27 On: Thu, 08 Oct 2015 04:16:26

# Transition in electron scattering mechanism in atomic layer deposited Nb:$TiO_2$ thin films

Janne-Petteri Niemelä,[1] Yasushi Hirose,[2,3,4] Tetsuya Hasegawa,[2,3,4] and Maarit Karppinen[1,a)]
[1]*Department of Chemistry, Aalto University, FI-00076 Aalto, Finland*
[2]*Department of Chemistry, The University of Tokyo, Tokyo 113-0033, Japan*
[3]*Kanagawa Academy of Science and Technology, Kawasaki 213-0012, Japan*
[4]*CREST, Japan Science and Technology Agency, Tokyo 113-0033, Japan*

(Received 19 December 2014; accepted 15 January 2015; published online 26 January 2015)

We characterized transport and optical properties of atomic layer deposited Nb:$TiO_2$ thin films on glass substrates. These promising transparent conducting oxide (TCO) materials show minimum resistivity of $1.0 \times 10^{-3}\,\Omega\,\text{cm}$ at 300 K and high transmittance in the visible range. Low-temperature (2–300 K) Hall measurements and the Drude fitting of the Vis-NIR optical spectra indicate a transition in the scattering mechanism from grain boundary scattering to intra-grain scattering with increasing Nb content, thus underlining enhancement of the grain size in the low doping regime as the key for further improved TCO properties. © *2015 AIP Publishing LLC*.
[http://dx.doi.org/10.1063/1.4906865]

Niobium-doped anatase $TiO_2$ is a wide-gap n-type semiconductor, which allows for high transmittance in the visible range of light with its fundamental absorption edge lying above 3.2 eV.[1] As pentavalent niobium is well soluble in the anatase lattice, carrier electron densities even higher than $10^{21}\,\text{cm}^{-3}$ can be doped into the conduction band of Nb:$TiO_2$, and consequently, resistivity values as low as $\sim 2\text{–}4 \times 10^{-4}\,\Omega\,\text{cm}$ can be reached for epitaxial films.[2,3] Such a combination of high transmittance and high electrical conductivity makes Nb:$TiO_2$ a promising candidate for a transparent conducting oxide (TCO) material to challenge the more common TCO materials, Sn:$In_2O_3$ and Al:ZnO. Potential applications for Nb:$TiO_2$ include, e.g., solar cells and blue LEDs where the unique characteristics of Nb:$TiO_2$, that is, the high refractive index and the high IR-transmittance could be exploited.[4]

For practical applications, a technique is required, which would enable the deposition of low-resistivity Nb:$TiO_2$ thin films even on large-area glass substrates. Atomic layer deposition (ALD) is an industrially feasible thin-film fabrication technique, and the technique of choice when homogeneous pinhole-free oxide or sulphide thin films on large-area substrates are demanded.[5] What comes to TCO materials, for instance, high-quality thin films of Sn:$In_2O_3$ and Al:ZnO with room-temperature (RT) resistivity values of the order of $10^{-4}\,\Omega\,\text{cm}$ have been fabricated with ALD.[6–8] Moreover, uniquely to ALD, the self-limiting nature of the film growth enables fabrication of conformal thin films even on complex nanostructures, a capability that is of increasing interest for future applications.[9] Another exciting aspect is that—potentially—the properties of ALD-fabricated thin films may be further tailored by introducing additional organic layers within the inorganic thin-film matrix by combining ALD cycles with molecular layer deposition (MLD) cycles based on organic precursors[10] to fabricate, e.g., hybrid oxide-organic superlattices.[11,12]

An appreciably low RT resistivity value of $\sim 1 \times 10^{-3}\,\Omega\,\text{cm}$ was recently achieved for ALD-fabricated $Ti_{1-x}Nb_xO_2$ films.[13,14] The best conductivity values were realized for the heavily doped films with $x > 0.2$, while for films fabricated by PLD or sputtering techniques electrical conductivity is typically maximized at $x \approx 0.05$. In this paper, we will show that this is due to a transition in the scattering mechanism with increasing Nb content in the ALD-grown films.

A series of $Ti_{1-x}Nb_xO_2$ thin films were deposited from $TiCl_4$, $Nb(OEt)_5$ and $H_2O$ precursors in a Picosun R-100 reactor on borosilicate glass substrates at 210 °C as briefly described below, and in more detail in our previous work.[13] Atomic composition was measured with energy-dispersive X-ray spectroscopy (EDX; JEOL JED-2300) equipped with a scanning electron microscope (JEOL JSM7000F) as Nb/(Ti + Nb) = 0.04, 0.09, 0.13, 0.18, 0.20, 0.23, and 0.25. The EDX values compare well with the corresponding ALD cycle ratios, 0.05, 0.10, 0.15, 0.20, 0.22, 0.24, and 0.25; hence, in the following, with $x$ we refer to the ALD cycle ratio rather than the Nb content values determined with EDX to be consistent with our previous work.[13] Based on X-ray reflectivity (XRR; PANanalytical X'Pert Pro MPD diffractometer) data, 2000 ALD cycles resulted in 64.5–70.5 nm thick films. The as-deposited films were amorphous, with the exception of undoped $TiO_2$ and $x = 0.05$ samples, for both of which the crystal structure was identified as anatase $TiO_2$. A post-deposition anneal at 600 °C for 60 min in $H_2$ gas (ULVAC-RIKO, MILA-3000-UHV) was performed to crystallize the films for all the compositions and to remove any excess oxygen from the materials.

X-ray diffraction (XRD; Cu $K_\alpha$, Bruker AXS d8 discover with GADDS) patterns for our annealed $Ti_{1-x}Nb_xO_2$ films, recorded in symmetric $\theta/2\theta$ mode using a two-dimensional detector, are shown in Fig. S1.[15] The films are

a)Author to whom correspondence should be addressed. Electronic mail: maarit.karppinen@aalto.fi

 © 2015 AIP Publishing LLC

This article is copyrighted as indicated in the article. Reuse of AIP content is subject to the terms at: http://scitation.aip.org/termsconditions. Downloaded to IP: 130.233.216.27 On: Thu, 08 Oct 2015 04:16:26

of the pure anatase phase for $x \leq 0.24$, while for the $x = 0.25$ film an inclusion of a rutile impurity phase is seen. From the inset of Fig. S1, we can see that the unit cell volume increases linearly up to $x = 0.25$ and Nb indeed substitutes Ti in the anatase lattice. Finally, considering the texture of the films, we may conclude that the degree of *c*-axis orientation increases with Nb-doping for $x \geq 0.20$ and maximizes at $x = 0.24$, a beneficial fact that enables increased electron transport via high-mobility (*a,b*) plane in the anatase lattice.[16]

Optical properties of the $Ti_{1-x}Nb_xO_2$ films were investigated by measuring normal transmittance ($T$) and reflectance ($R$) spectra in the wavelength range of 250–2300 nm (Jasco V670 with ARN-731, incident angle 5°). In Fig. 1, we show the transmittance and absorbance ($A = 1 - T - R$) spectra as well as the $(\alpha h\nu)^{1/2}$ vs. $h\nu$ plots (where $\alpha$ is the absorption coefficient and $h\nu$ is the photon energy) for the determination of the fundamental absorption energies ($E_g$) and the obtained $E_g$ values as a function of $x$. The films show rather high transmittance in the visible range of approximately 70% on average. In the UV range, below ~400 nm, transmittance steeply drops to zero for all the films, whereas in the Vis-NIR range transmission of light becomes progressively reduced with increasing Nb content $x$ in the films (Fig. 1(a)). The reduced Vis-NIR transmittance can be ascribed to increased free carrier absorption with increasing $x$ that causes a particularly negative effect in the higher doping regime of $x > 0.15$, affecting the transparency of the films even in the visible range (Fig. 1(b)). The small peak in absorbance around 400 nm indicates the presence of some unexpected impurities for undoped $TiO_2$ ($x = 0.00$), whereas the slightly reduced IR absorption for the $x = 0.25$ film could be ascribed to the rutile impurity. Note that we do not see any sign of free carrier absorption for the as-deposited films, which indicates that the electrons from Nb are released to the conduction band of $TiO_2$ upon the post-deposition annealing step.

The steep drop seen in transmittance below 400 nm is caused by the band-gap absorption. As determined from the $(\alpha h\nu)^{1/2}$ vs. $h\nu$ plots, the fundamental absorption energy values shift towards higher energies with Nb doping from around 3.3 eV for the undoped film to around 3.5 eV for films with $0.05 \leq x \leq 0.24$ (Figs. 1(c) and 1(d)). Such a shift can most probably be ascribed to a Fermi-level rise inside the conduction band with increasing $x$, often seen for degenerate semiconductors. The slight drop in the $E_g$ values for $0.20 \leq x \leq 0.24$ can be due to band-gap narrowing ascribed to electron-electron and electron-ion scattering for such heavily doped materials and anisotropy in the optical gap starting to affect with increasing *c*-axis orientation.[17,18] The further drop seen for the $x = 0.25$ film is an effect originating from the appearance of the rutile phase with a smaller band gap (~3.0 eV) than that of anatase $TiO_2$ (~3.2 eV).[1] To sum up, by doping our anatase $TiO_2$ films with Nb, their transparency window is extended slightly in the UV region, whereas a drawback of reduced transparency is seen in the Vis-NIR region, particularly in the high doping regime of $x > 0.15$.

Electronic transport properties of the films were studied by measuring the Hall effect in Van der Pauw configuration in the temperature range of 2–300 K (Quantum Design Physical Property Measurement System; ±9 T magnetic flux density). Four copper wires attached with indium to silver contacts evaporated on the sample corners were used to form the electrical contacts with the film surface. Conductivity is notably enhanced with increasing Nb content, the RT resistivity value decreasing from $4.5 \times 10^{-1}\,\Omega\,\text{cm}$ at $x = 0$ to $1.0 \times 10^{-3}\,\Omega\,\text{cm}$ at $x = 0.22$ (Fig. 2(a)). Further increase in the Nb content beyond $x = 0.24$ results in a sudden increase in resistivity for the $x = 0.25$ film, most probably due to inclusions of the high-resistivity rutile phase.[1] The resistivity values depend moderately on temperature such that for $x \leq 0.15$ and $x = 0.25$ resistivity decreases with increasing

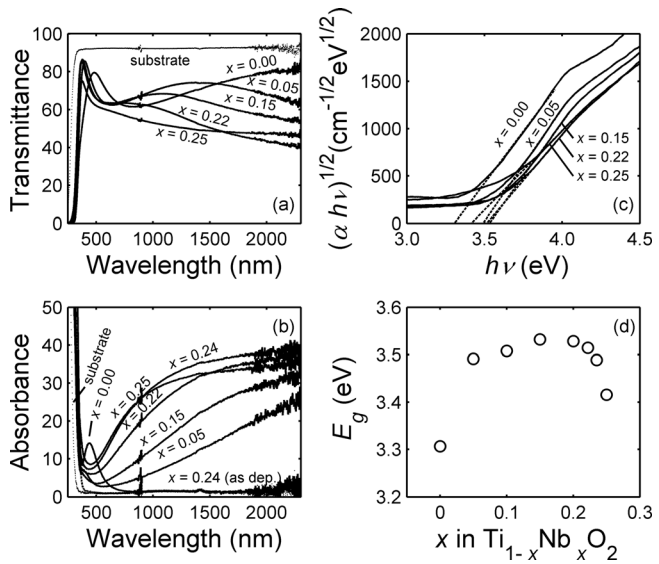


FIG. 1. UV-Vis-NIR (a) transmittance and (b) absorbance for selected $Ti_{1-x}Nb_xO_2$ films annealed at 600 °C in $H_2$, together with (c) illustrative $(\alpha h\nu)^{1/2}$ vs. $h\nu$ plots, where $\alpha$ is the absorption coefficient and $h\nu$ the photon energy, and (d) fundamental absorption energies $E_g$. In addition to the spectra for the annealed films, image (b) shows the absorbance spectrum for the as-deposited $x = 0.24$ film.

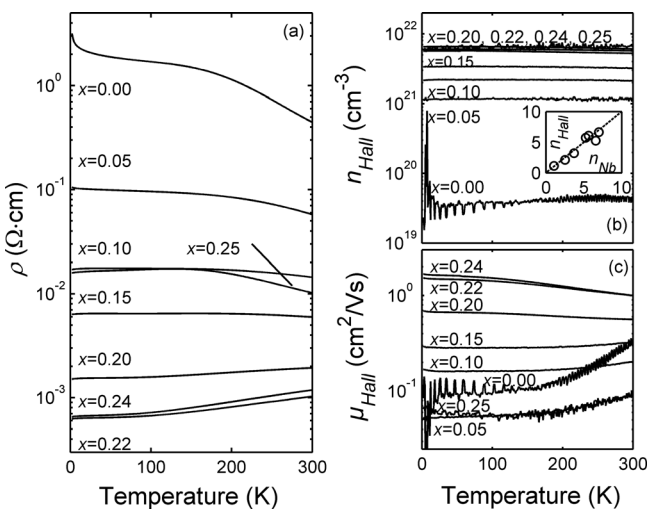


FIG. 2. Results of Hall effect measurements for the $Ti_{1-x}Nb_xO_2$ films in the temperature range of 2–300 K: (a) resistivity $\rho$, (b) carrier density $n_{Hall}$, and (c) mobility $\mu_{Hall}$. In the inset of image (b) shown are the carrier electron density $n_{Hall}$ ($\times 10^{21}\,\text{cm}^{-3}$) as a function of Nb atomic density $n_{Nb}$ ($\times 10^{21}\,\text{cm}^{-3}$) and a line that represents 100% ionization efficiency.

This article is copyrighted as indicated in the article. Reuse of AIP content is subject to the terms at: http://scitation.aip.org/termsconditions. Downloaded to IP: 130.233.216.27 On: Thu, 08 Oct 2015 04:16:26

temperature, whereas for $0.20 \leq x \leq 0.24$ an opposite trend of increasing resistivity is observed.

In line with the notably reduced RT resistivity values, and the absorbance spectra shown in Fig. 2(b), Nb-for-Ti substitution yields an increase in the carrier density value $n_{Hall}$ from $4.2 \times 10^{19}\,\mathrm{cm}^{-3}$ for $TiO_2$ to a maximum of $6.7 \times 10^{21}\,\mathrm{cm}^{-3}$ for $x = 0.25$ at 300 K (Fig. 2(b)). It is of note that the $n_{Hall}$ values for all the doped samples are high resulting in high ionization efficiency values for Nb close to 100%, as is shown in the inset of Fig. 2(b). For undoped $TiO_2$ an indication of slight temperature activation of conduction electrons is observed as $n_{Hall}$ increases moderately over the measured temperature range, whereas all the doped samples show essentially flat temperature profiles, that is, the Nb-substituted films behave as degenerate semiconductors.

The RT Hall mobility $\mu_{Hall}$ value for undoped $TiO_2$, *i.e.*, $0.33\,\mathrm{cm}^2/\mathrm{Vs}$, at first decreases by doping to a value of $0.20\,\mathrm{cm}^2/\mathrm{Vs}$ for $x = 0.05$, and then increases for the higher substitution levels of $x \geq 10$ reaching a maximum value of $1.1\,\mathrm{cm}^2/\mathrm{Vs}$ for $x = 0.22$, finally lowering again for the $x = 0.25$ film with rutile inclusions (Fig. 2(c)). The temperature dependencies of the $\mu_{Hall}$ values reflect the corresponding dependencies on the resistivity values, as expected from the essentially flat carrier density profiles. For $0.20 \leq x \leq 0.24$, the increasing trend with decreasing temperature indicates phonon-limited electron transport, whereas for $x \leq 0.15$ the sign of the slope of the curves changes from negative to positive implying that in this regime of lower doping charge transport is predominately limited by a mechanism other than intra-grain phonon scattering.[19] Another possible intra-grain scattering source could be neutral and ionized impurities, that is, mainly Nb ions in the highly-doped Nb:$TiO_2$ samples. Scattering from such point defects should have a reducing effect on mobility with increasing amount of impurities; however, the finding that $\mu_{Hall}$ increases with increasing $x$ for $0.05 \leq x \leq 0.24$ rules out this possibility and rather implies that the dominating scattering source for $x \leq 0.15$ would be grain boundaries, hence of inter-grain nature. The low mobility in the $x = 0.25$ film can be ascribed to the presence of rutile phase with a high effective mass of $\sim 20\, m_e$ for conduction electrons.[20]

In the Hall effect measurement, the conduction electrons are transported over macroscopic distances, and thus, for polycrystalline materials, the electrons are subject to grain boundary scattering, which is reflected in the $\mu_{Hall}$ values at sufficiently high grain boundary densities. On the other hand, if the electron mobility is determined by optical means, the average electron paths under rapidly oscillating electric fields of the incident light are typically smaller than the average grain size, and the obtained mobility values are mainly sensitive to intra-grain scattering. Hence, a comparison of the optical and Hall mobility values can reveal whether charge transport is predominately limited by scattering in the bulk of the grains or at the boundaries between the grains.[21,22]

The optical mobility $\mu_{opt}$ values can be determined by fitting measured reflectance and transmittance spectra in the Vis-NIR wavelength range where free carrier absorption takes place. Transmittance and reflectance of a thin film are essentially determined by the complex dielectric function $\varepsilon$ of the film material, described in a simple way for a material with free carrier absorption by the Drude model as[21]

$$\varepsilon(\omega) = \varepsilon_\infty[1 - \omega_p^2/(\omega^2 - i\omega/\tau)], \tag{1}$$

where $\omega$ is the angular frequency, $\varepsilon_\infty$ is the high frequency dielectric constant, and $i$ is the imaginary unit. The plasma frequency $\omega_p$ depends essentially on carrier electron density $n$ and electron effective mass $m^*$ as

$$\omega_p = \sqrt{(ne^2)/(\varepsilon_\infty \varepsilon_0 m^*)}, \tag{2}$$

where $e$ is the electron charge and $\varepsilon_0$ is the permittivity of vacuum. Finally, the information on optical mobility $\mu_{opt}$ is contained in the following equation for the scattering time $\tau$:

$$\tau = \mu_{opt} m^*/e. \tag{3}$$

We estimate the $\mu_{opt}$ values by fitting the model described above, including the effect of the multiple reflections within the air/film/substrate stack, to the measured Vis-NIR reflectance and transmittance spectra using $m^*$ and $\tau$ as fitting parameters. Carrier densities are obtained from the Hall measurement data and for $\varepsilon_\infty$ a literature value of 5.9[23] is used for $0.05 \leq x \leq 0.15$. Lowering $\varepsilon_\infty$ to 5.7 for $x = 0.20$ and 0.22, and to 5.5 for $x = 0.24$ and 0.25 slightly improves the fit. Altogether, an excellent fit between the theory and the experiment is obtained, as is seen in Fig. 3(a) for $x = 0.05$ and 0.24 as selected examples. The fitting parameters show reasonable trends as $m^*$ first increases with increasing $x$ up to $x = 0.20$ reflecting non-parabolicity of the conduction band,[19] and then decreases for $0.20 \leq x \leq 0.24$ where movement of the electrons along the low-effective-mass $(a,b)$ plane becomes significant as a result of increased $c$-axis orientation of the crystallites (see Figs. S1 and 3(b)). For the $x = 0.25$ film, $m^*$ increases as a consequence of the rutile inclusions. In addition, the scattering time is found to decrease monotonously with increasing $x$, which is expected

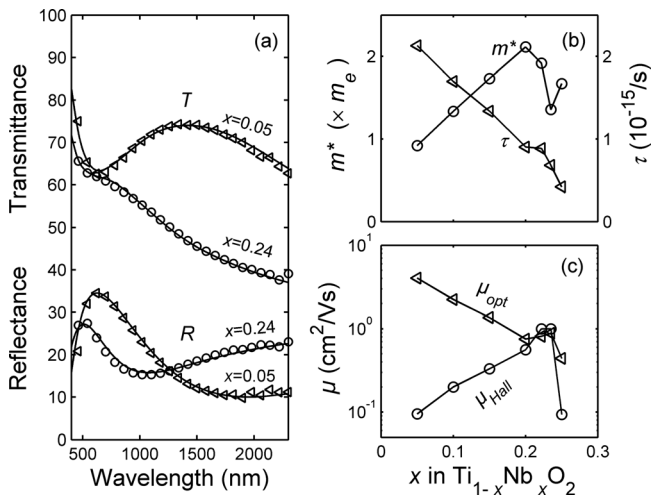


FIG. 3. Drude fitting of the transmittance $T$ and reflectance $R$ spectra of the $Ti_{1-x}Nb_xO_2$ films in the wavelength range of 400–2300 nm: (a) spectra for the selected $x = 0.05$ and 0.24 films (symbols) and the respective fits (lines), (b) values of the fitting parameters, the effective electron mass $m^*$ and the scattering time $\tau$, for $0.05 \leq x \leq 0.25$, and (c) comparison of the obtained $\mu_{opt}$ and $\mu_{Hall}$ values for $0.05 \leq x \leq 0.25$.

This article is copyrighted as indicated in the article. Reuse of AIP content is subject to the terms at: http://scitation.aip.org/termsconditions. Downloaded to IP: 130.233.216.27 On: Thu, 08 Oct 2015 04:16:26

from the increasing density of the scattering centers formed by the Nb ions, and particularly, from the reducing effect of phonon contribution to the total mobility with increasing $x$ (Fig. 3(b)).[19] The $\mu_{opt}$ values calculated from Eq. (3) can be explained in terms of the trends seen for the fitting parameters $m^*$ and $\tau$ (Fig. 3(c)). As $x$ increases from 0.05 to 0.20, the reduction for $\tau$ out weights the impact of increasing $m^*$ and $\mu_{opt}$ reduces, whereas for $0.20 \leq x \leq 0.24$, the notable drop in $m^*$ due to enhanced $c$-axis orientation of the film results in an increase in $\mu_{opt}$. For $x = 0.25$, the rutile inclusions yield reduced $\mu_{opt}$ values. Most importantly, the $\mu_{opt}$ values are notably larger than the $\mu_{Hall}$ values for $x \leq 0.15$ and become similar for $0.20 \leq x \leq 0.24$. This indicates that, in agreement with the temperature dependencies of the Hall measurement data, the electron mobility in our anatase $Ti_{1-x}Nb_xO_2$ thin films is predominately limited by grain boundary scattering in the lower substitution regime $x < 0.20$ and by intra-grain scattering in the higher substitution regime $0.20 \leq x \leq 0.24$. The reasoning is justified as the electron mean free paths calculated from the $\mu_{opt}$ values remain below nm, that is, notably below the typical grain size. Moreover, the obtained $\mu_{opt}$ values are reasonable, though, lower than the phonon limited (intra-grain scattering limited) $\mu_{Hall}$ values for epitaxial films, *e.g.*, for $x \approx 0.05$ $\mu_{opt} = 4.0\,cm^2/Vs$ for our film with random orientation and $\mu_{Hall} \approx 20\,cm^2/Vs$ for epitaxial $c$-axis oriented film.[19] These mobility values become comparable once the anisotropy in the effective mass, $3\,m^*_{a,b} \leq m^*_c \leq 6\,m^*_{a,b}$, is considered.[16]

In order to support the results of the Hall and optical mobility analysis, the present $Ti_{1-x}Nb_xO_2$ films were imaged by means of polarized light microscopy (PLM; Olympus BX50) and scanning electron microscopy (SEM; JEOL JSM7000F) (Fig. S2).[15] The results of the PLM imaging indicate a clear transition in crystallinity between the $x$ values 0.15 and 0.20: for $x \leq 0.15$, the surface images are featureless, whereas for $x \geq 0.20$ grains with size of tens of micrometers are clearly observed (Fig. S2, top). The images with higher magnification obtained with SEM reveal that the grain size is of the order of 1 $\mu$m or below for $x \leq 0.15$ (Fig. S2, middle). In this substitution regime also some cracks, which could have a lowering effect on the mobility values, are observed. Pore *et al.* showed that highly-substituted $Ti_{1-x}Nb_xO_2$ films exhibit large and essentially $c$-axis oriented grains spanned by cross-shaped features, where the arms of the crosses were identified as domains of single-crystalline $c$-axis-oriented anatase, and the wavy features as dislocations or very small cracks with the orientation differing not more than $\sim 2^\circ$ from the $c$-axis oriented arms.[14] For the present films, we could indeed confirm presence of such $c$-axis oriented cross shapes for the films with $x \geq 0.20$.[15] Altogether, the change in crystallinity around $x \sim 0.15$–$0.20$ is in line with the observations from the Hall and optical mobility analysis, that is, grain boundary scattering limits electronic conductivity for $x \leq 0.15$, whereas phonon scattering is the dominating mechanism for $0.20 \leq x \leq 0.24$.

In conclusion, we find the anatase $Ti_{1-x}Nb_xO_2$ thin films fabricated by ALD as promising TCO materials, particularly for applications where large-area depositions and conformal coatings on nanostructures are required. However, optical transmittance and electrical conductivity are not simultaneously optimized: conductivity is high in the high doping regime, whereas in the low doping regime where transmittance is high, the films suffer from low conductivity. Here, we have shown that this contradiction stems from a transition in the scattering mechanism from phonon scattering dominating in the high doping regime to grain boundary scattering that is found to substantially limit the electron transport in the low doping regime. Enhancing the electron mobility by increasing the grain size in the low doping regime is hence the key to improve the TCO properties of the ALD-fabricated $Ti_{1-x}Nb_xO_2$ films further.

The present work has received funding from the European Research Council under the European Union's Seventh Framework Programme (FP/2007-2013)/ERC Advanced Grant Agreement (No. 339478), the Aalto Energy Efficiency Research Programme, and the Scandinavia-Japan Sasakawa Foundation.

[1]S. X. Zhang, D. C. Kundaliya, W. Yu, S. Dhar, S. Y. Young, L. G. Salamanca-Riba, S. B. Ogale, R. D. Vispute, and T. Venkatesan, J. Appl. Phys. **102**, 013701 (2007).
[2]Y. Furubayashi, T. Hitosugi, Y. Yamamoto, K. Inaba, G. Kinoda, Y. Hirose, T. Shimada, and T. Hasegawa, Appl. Phys. Lett. **86**, 252101 (2005).
[3]M. A. Gillispie, M. F. A. M. van Hest, M. S. Dabney, J. D. Perkins, and D. S. Ginley, J. Appl. Phys. **101**, 033125 (2007).
[4]T. Hitosugi, N. Yamada, S. Nakao, Y. Hirose, and T. Hasegawa, Phys. Status Solidi A **207**, 1529–1537 (2010).
[5]V. Miikkulainen, M. Leskelä, M. Ritala, and R. L. Puurunen, J. Appl. Phys. **113**, 021301 (2013).
[6]M. Ritala, T. Asikainen, and M. Leskelä, Electrochem. Solid State Lett. **1**(3), 156–157 (1998).
[7]K. S. An, W. Cho, B. K. Lee, S. S. Lee, and C. G. Kim, J. Nanosci. Nanotechnol. **8**, 4856–4859 (2008).
[8]T. Tynell and M. Karppinen, Semicond. Sci. Technol. **29**, 043001 (2014).
[9]M. Knez, K. Nielsch, and L. Niinistö, Adv. Mater. **19**, 3425–3438 (2007).
[10]P. Sundberg and M. Karppinen, Beilstein J. Nanotechnol. **5**, 1104–1136 (2014).
[11]J.-P. Niemelä and M. Karppinen, Dalton Trans. **44**, 591–597 (2015).
[12]T. Tynell, I. Terasaki, H. Yamauchi, and M. Karppinen, J. Mater. Chem. A **1**, 13619–13624 (2013).
[13]J.-P. Niemelä, H. Yamauchi, and M. Karppinen, Thin Solid Films **551**, 19–22 (2014).
[14]V. Pore, M. Ritala, M. Leskelä, T. Saukkonen, and M. Järn, Cryst. Growth Des. **9**, 2974–2978 (2009).
[15]See supplementary material at http://dx.doi.org/10.1063/1.4906865 for XRD patterns as well as for PLM and SEM images.
[16]Y. Hirose, N. Yamada, S. Nakao, T. Hitosugi, T. Shimada, and T. Hasegawa, Phys. Rev. B **79**, 165108 (2009).
[17]B. E. Sernelius, K.-F. Berggren, Z.-C. Jin, I. Hamberg, and C. G. Granvqvist, Phys. Rev. B **37**(17), 10244–10248 (1988).
[18]H. Tang, F. Lévy, H. Berger, and P. E. Schmid, Phys. Rev. B **52**(11), 7771–7774 (1995).
[19]Y. Furubayashi, N. Yamada, Y. Hirose, Y. Yamamoto, M. Otani, T. Hitosugi, T. Shimada, and T. Hasegawa, J. Appl. Phys. **101**, 093705 (2007).
[20]H. P. R. Frederikse, J. Appl. Phys. **32**, 2211–2215 (1961).
[21]*Handbook of Transparent Conductors*, edited by D. S. Ginley, H. Hosono, and D. C. Paine (Springer, 2010), pp. 52, 125.
[22]J. Steinhauser, S. Faÿ, N. Oliveira, E. Vallat-Sauvain, and C. Ballif, Appl. Phys. Lett. **90**, 142107 (2007).
[23]N. Hosaka, T. Sekiya, C. Satoko, and S. Kurita, J. Phys. Soc. Jpn. **66**, 877–880 (1997).

This article is copyrighted as indicated in the article. Reuse of AIP content is subject to the terms at: http://scitation.aip.org/termsconditions. Downloaded to IP: 130.233.216.27 On: Thu, 08 Oct 2015 04:16:26